Sonic Horizon and Sub-sonic structure of Wolf-Rayet stars

Constraints on the mass-loss rates of WNE stars

Argelander-Institut für Astronomie

Luca Grassitelli

N.Langer, N.J.Grin, J.Mackey, J.M.Bestenlehner, G.Graefener

UNIVERSITÄT BONN

Wolf-Rayet Phenomenon:

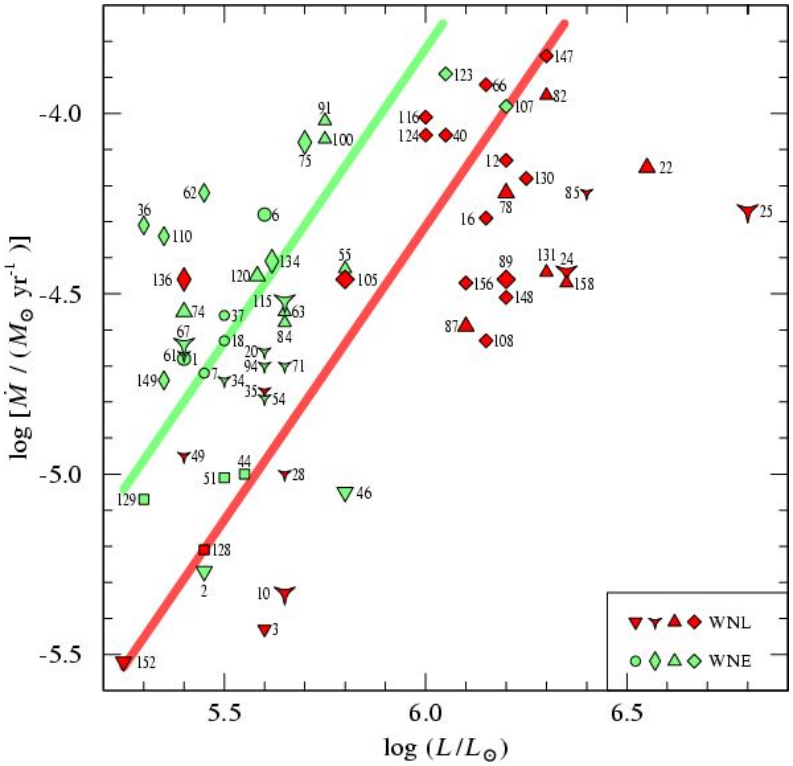

Empirical mass-loss rates Vs luminosity for the Galactic WN stars. Red: WNL stars, Green: WNE stars. *Hamann et al.2006*

- **spectra dominated by broad emission lines of He, C, N, O**
- **dense, optically thick stellar winds due to the high mass-loss rates**
- **naked cores in the final phases of the evolution of massive stars**

- enrich the interstellar medium
- SNe and GRBs progenitors
- physics of stellar winds

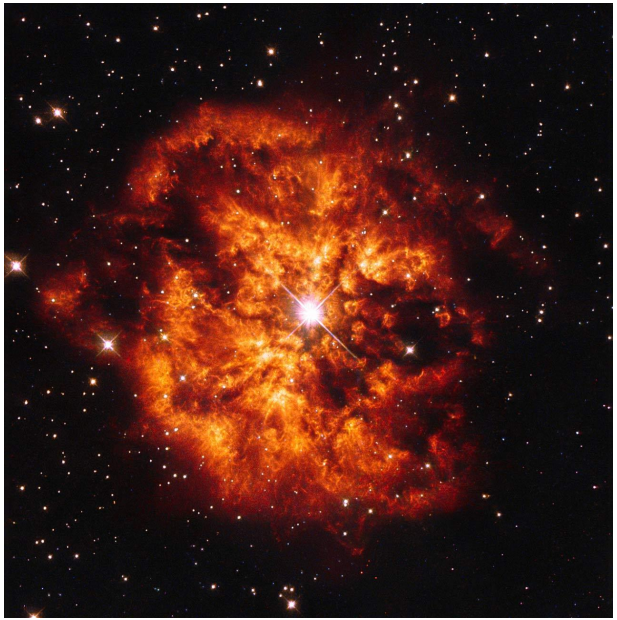

Hubble image shows the nebula M1-67 around the Wolf-Rayet star WR 124

WR radius problem:

Radii estimated via spectroscopy and wind models

(adopting a beta-velocity law)

≠

Radii stellar structure models

(hydrostatic with plane parallel atmosphere)

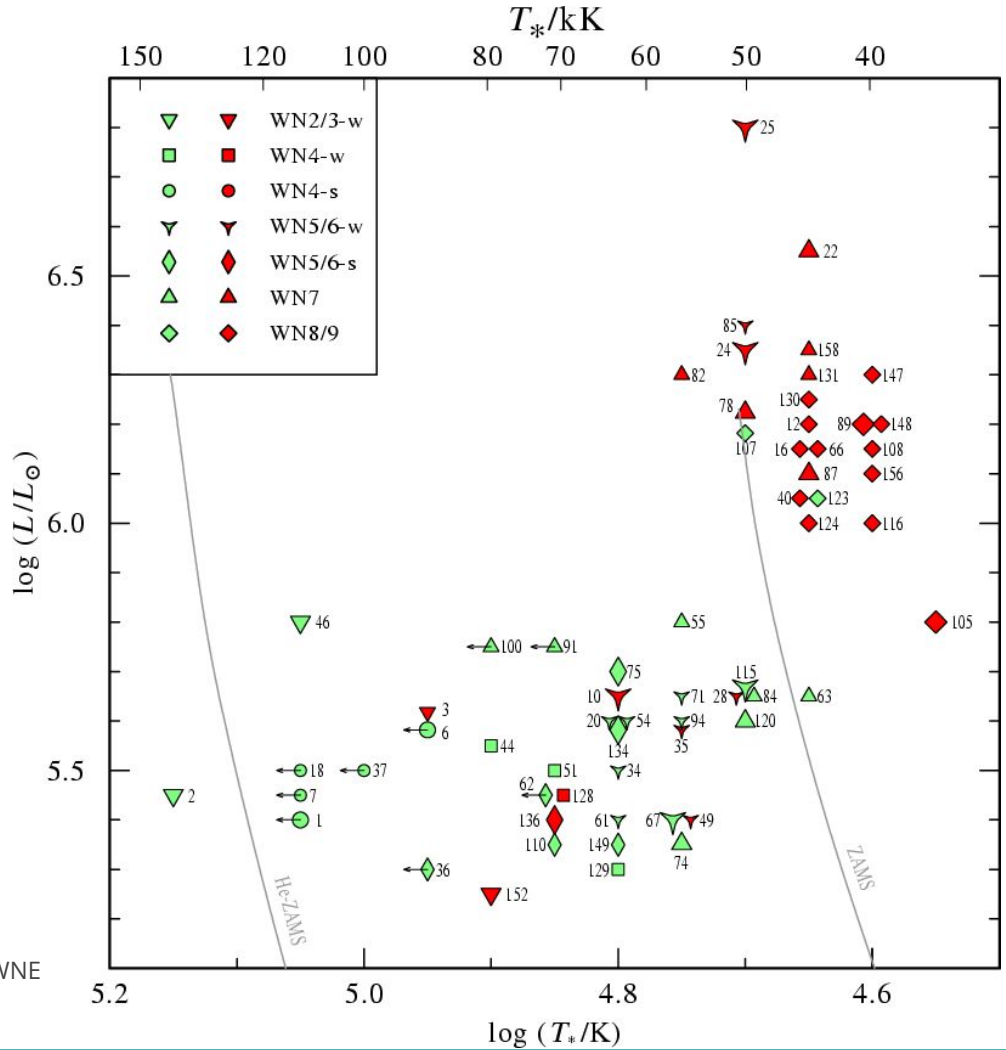

Figure: HR diagram with the WNL and WNE stars (T* temp. at τ=20). *Hamann et al.2006*

Dynamics of a steady-state stellar winds

$$\frac{1}{v}\frac{dv}{dr} = -\left(g - g_{rad} - 2\frac{c_s^2}{r} + \frac{dc_s^2}{dr}\right)/(v^2 - c_s^2)$$

critical point: $v = c_s$

Radiation driven winds:

$$g_{rad} \gg 2\frac{c_s^2}{r} - \frac{dc_s^2}{dr}$$

$$\frac{d\kappa}{dr} > 0$$ at the sonic point

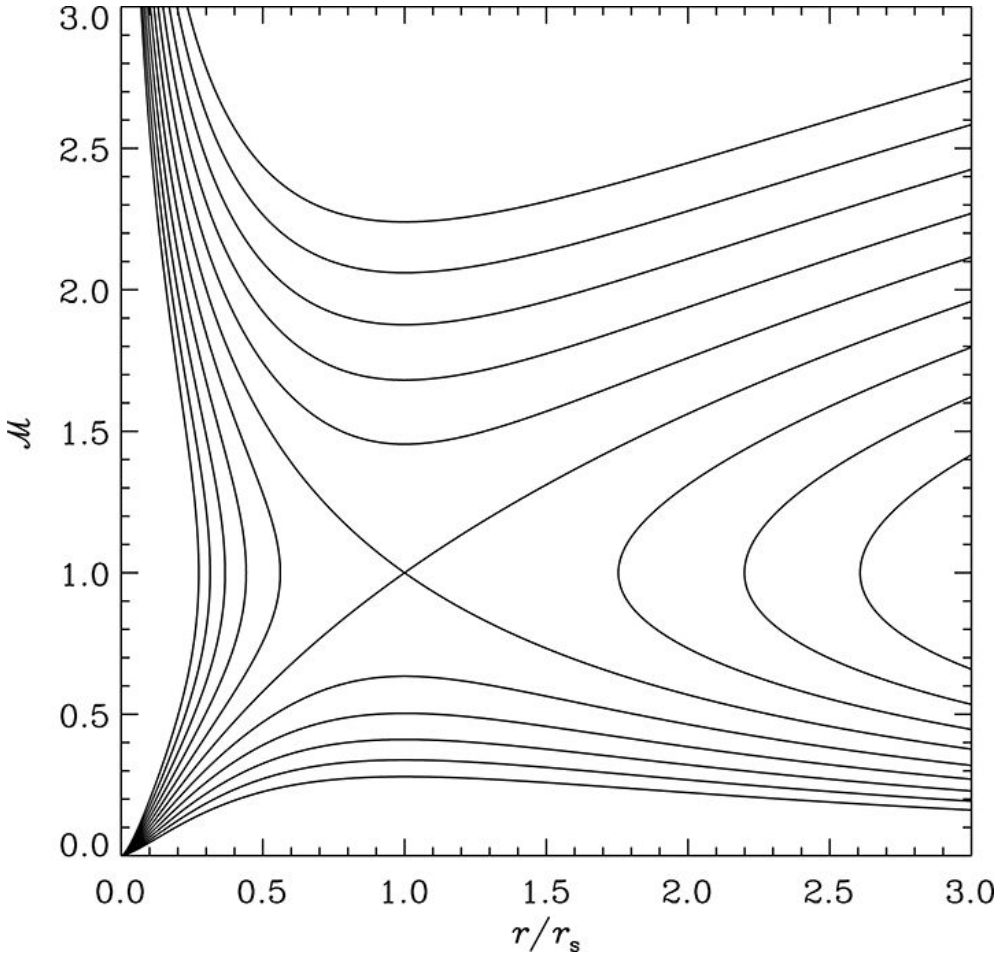

Figure: Solution curves for a stellar wind or accretion flow. X -type critical point at the sonic radius. *Ogilvie 2016*

The subsonic flow becomes a zone of silence

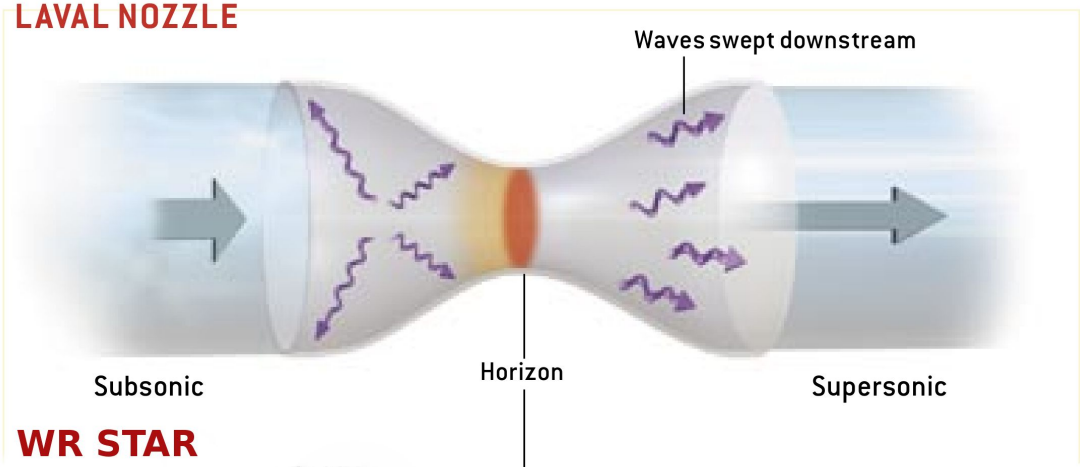

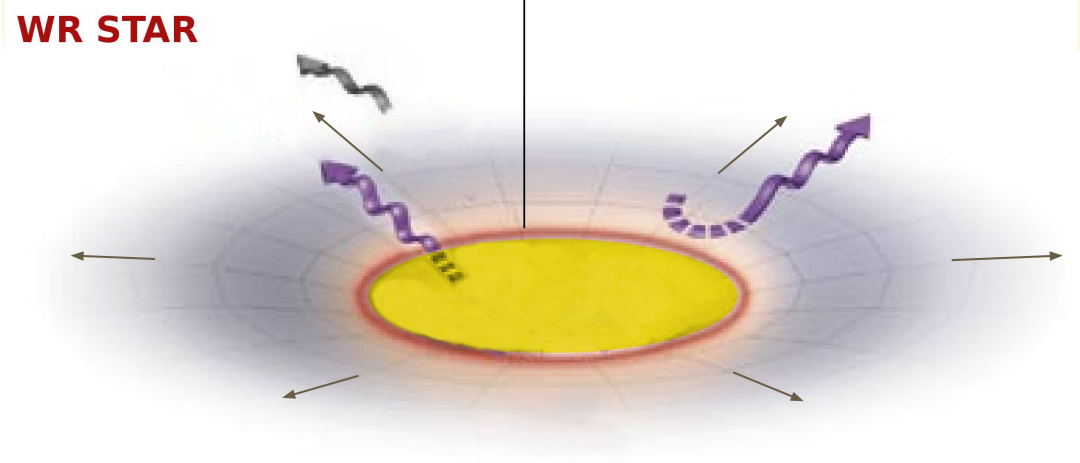

$$v > c_s$$

+

$$\lambda < H_p$$

$$\tau > 1$$

↓

Diffusive approximation ⇒ Properties of the radiation field can be described LOCALLY

BEC: Lagrangian 1D stellar evolution code

$$\left(\frac{\partial m}{\partial r}\right)_t = 4\pi r^2 \rho$$

$$\left(\frac{\partial r}{\partial t}\right)_m = v$$

$$\left(\frac{\partial L}{\partial m}\right)_t = \epsilon_N - \epsilon_g - \epsilon_\nu$$

$$\left(\frac{\partial T}{\partial m}\right)_t = -\frac{Gm}{4\pi r^4}\frac{T}{P}\nabla\left(1 + \frac{r^2}{Gm}\frac{\partial v}{\partial t}\right)_m$$

$$\left(\frac{a}{4\pi r^2}\right)_t = \frac{Gm}{4\pi r^4} + \frac{\partial P}{\partial m}$$

Surface boundary conditions

$$\dot{M} = 4\pi r^2 \rho v$$

$$v = \sqrt{\frac{k_B T}{\mu m_H}} = c_s$$

Massive Galactic Helium star models: 15 Msun

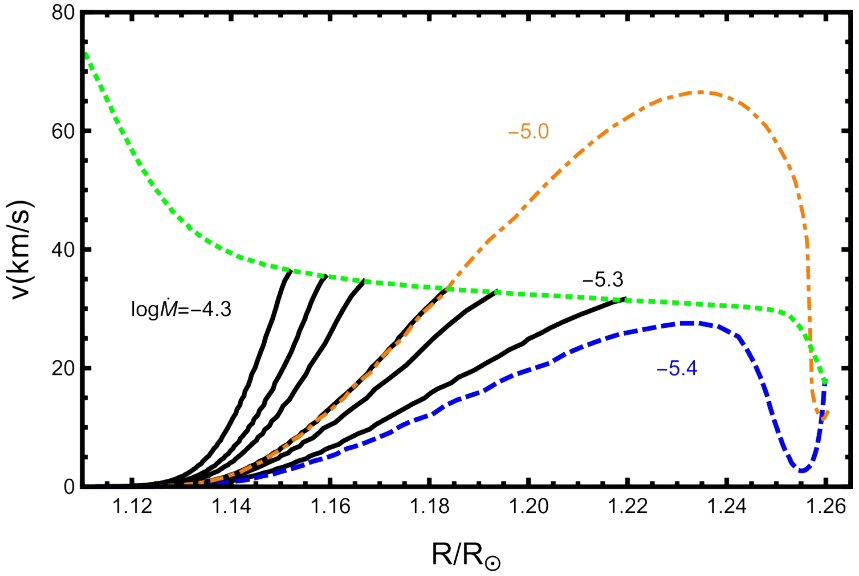

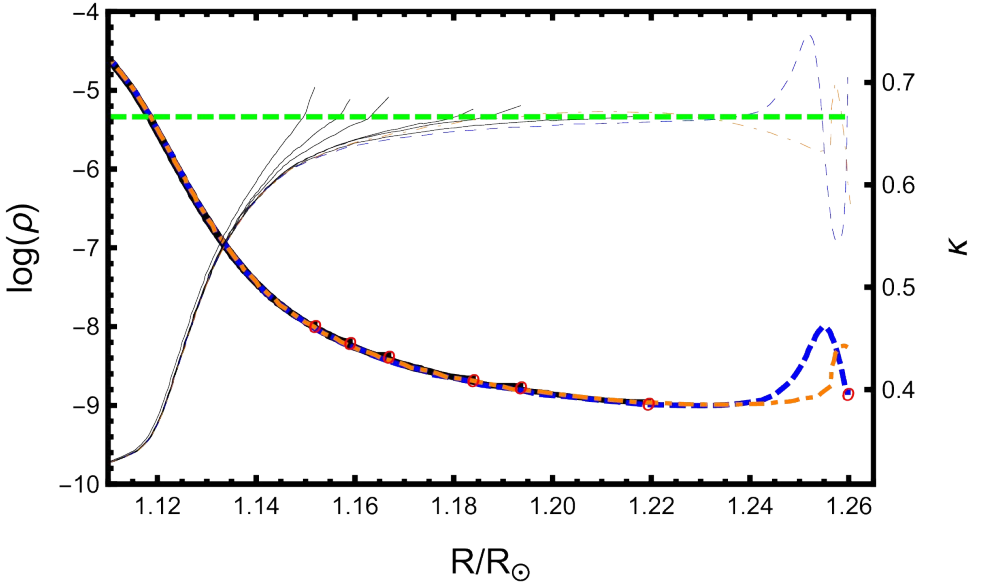

Black: Fe-bump, Blue: He-bump, Orange: plane-parallel atmosphere.
Green: isothermal sound speed.

As in Fig.Left. Green: Eddington opacity

$$\Gamma := \frac{g_{rad}}{g} = \frac{\kappa L}{4\pi c G M} \cong 1$$

log(ρ)-log(T)-K plane

for

$$\Gamma = \frac{\kappa}{4\pi cG}\frac{L}{M} = 1$$

$$\kappa_{edd} = 4\pi cG\frac{M}{L}$$

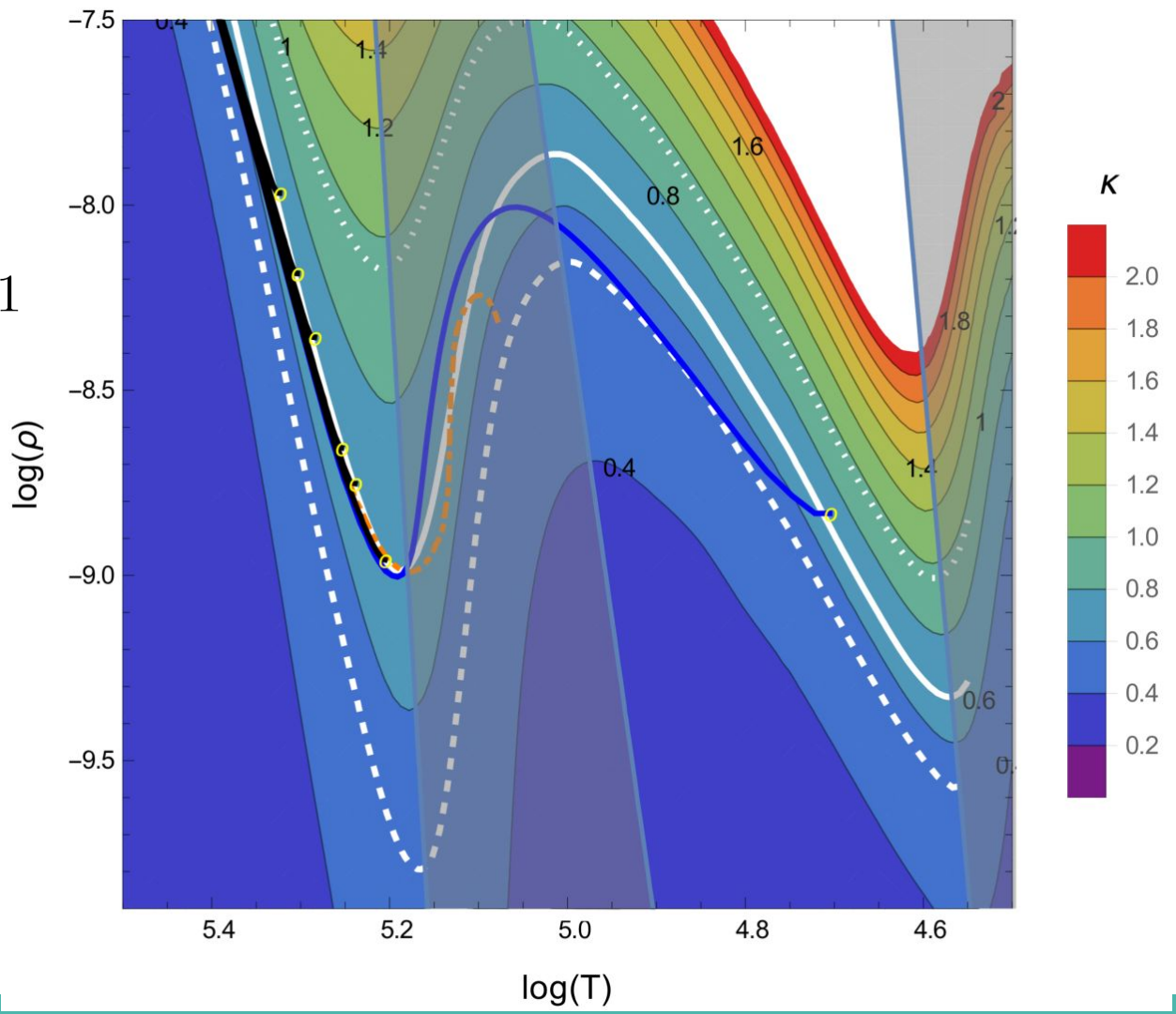

Sonic HR-diagram

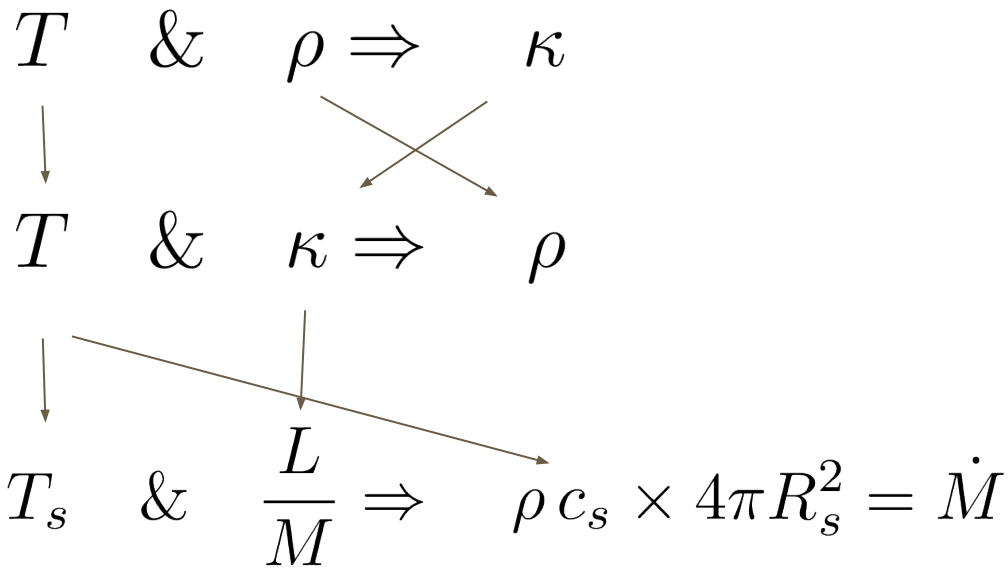

at the Sonic point:

Sonic HR-diagram

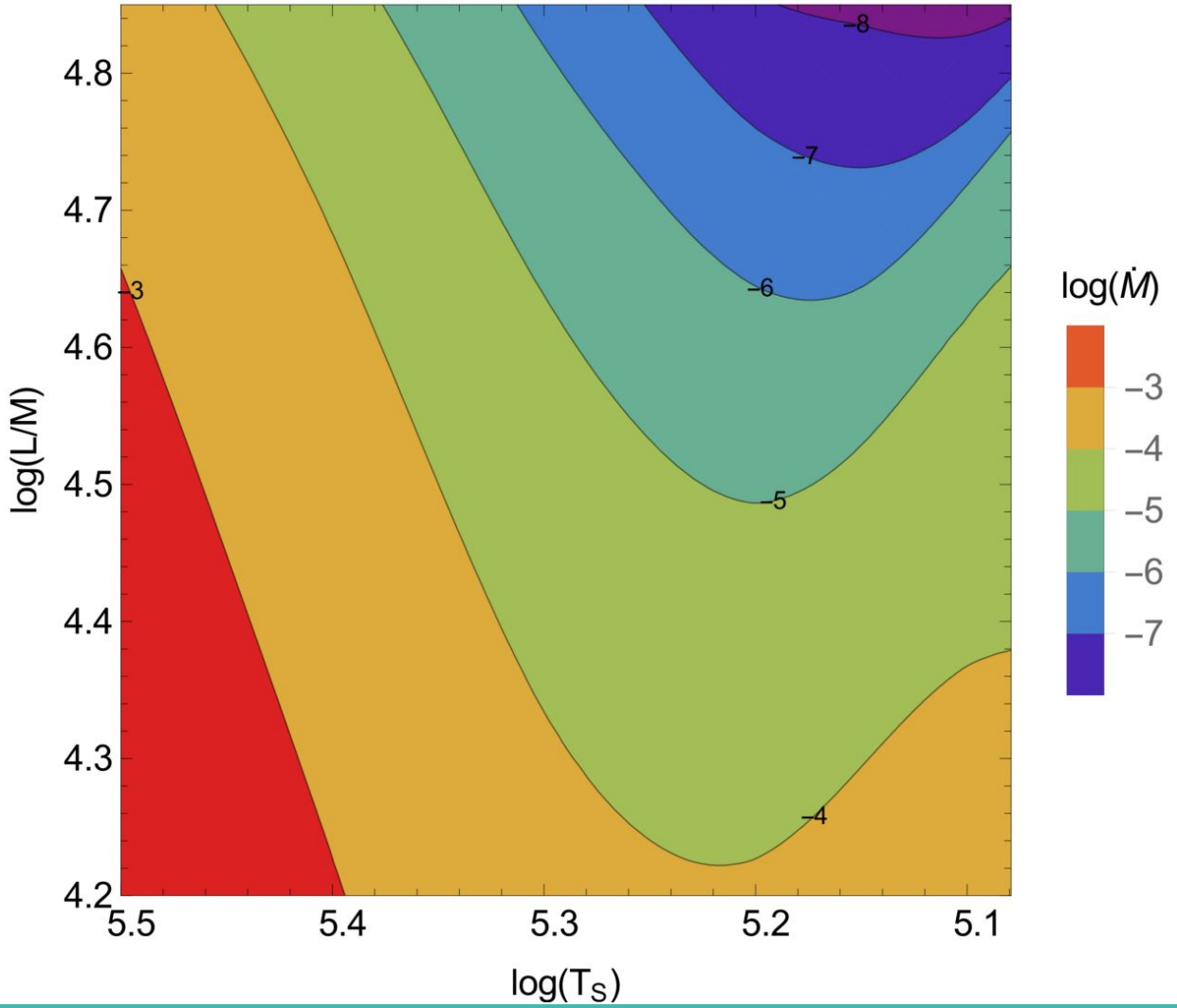

Minimum mass-loss rate

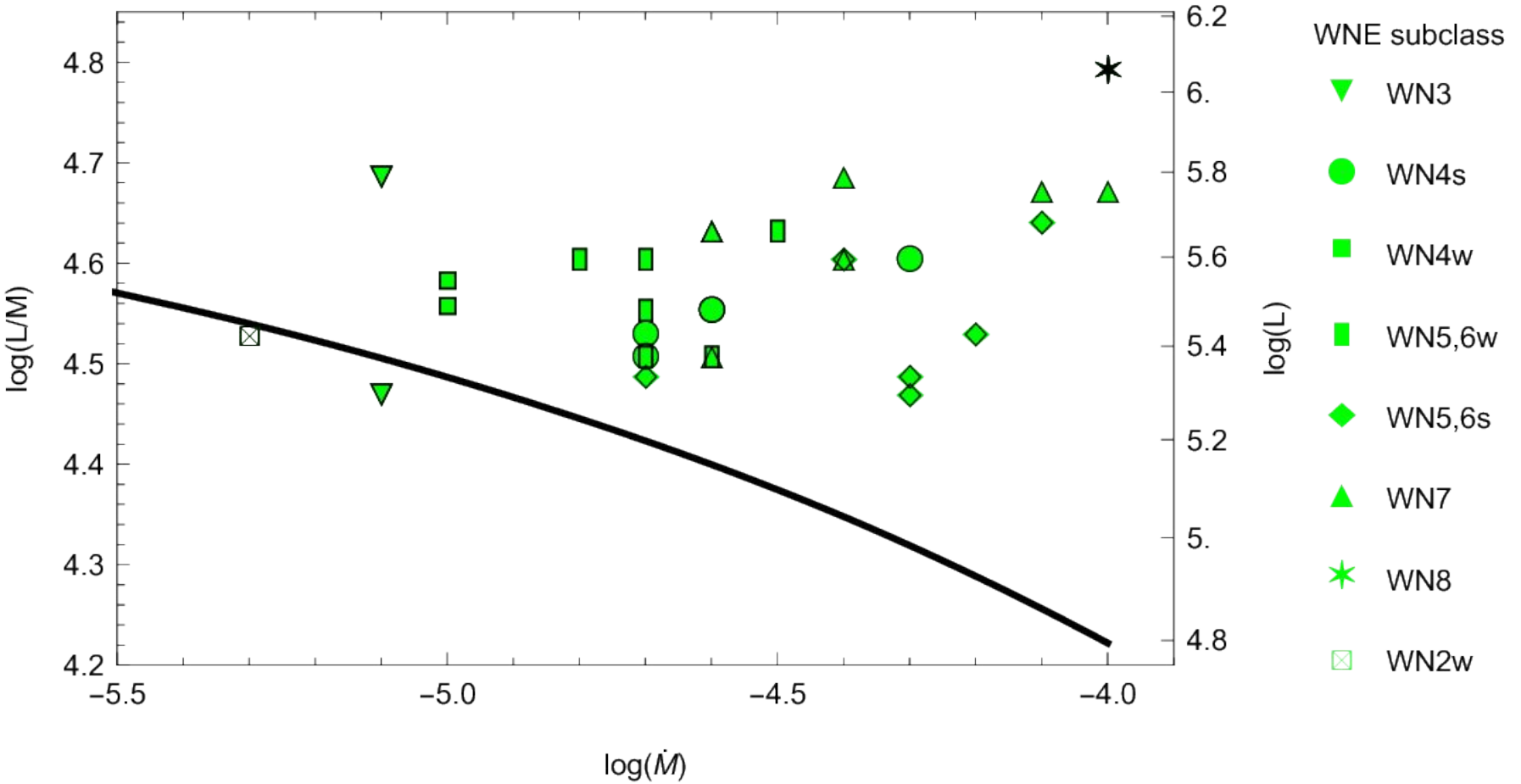

Sonic HR diagram

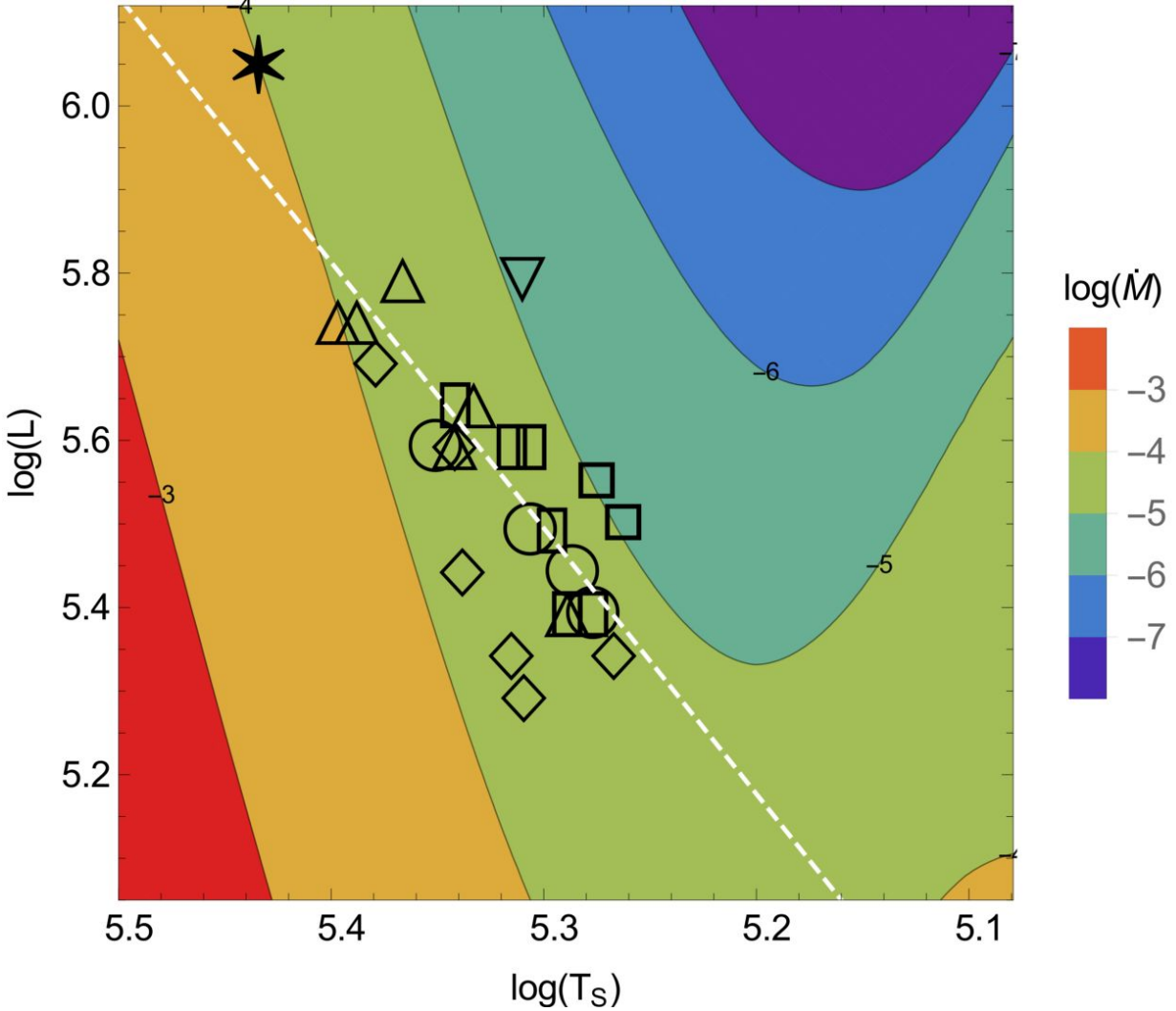

Conclusions

- Sonic Horizon allows to treat the subsonic structure and the optically thick wind separately
- Bifurcation Fe-bump and He-bump solutions
- Proximity of the sonic point to the Edd.limit ⇒ Sonic HR diagram
- Observed WNEs lie above the minimum Fe mass-loss rate ⇒ Flows driven by Fe bump
- WNE compact, ~ 1$R_\odot$ & 200kK, and our models can serve as inner boundary for atmosphere codes

WR radius problem ⟶ WR wind dynamics problem (stagnation?multiple crit.points?)

WR111, WC5

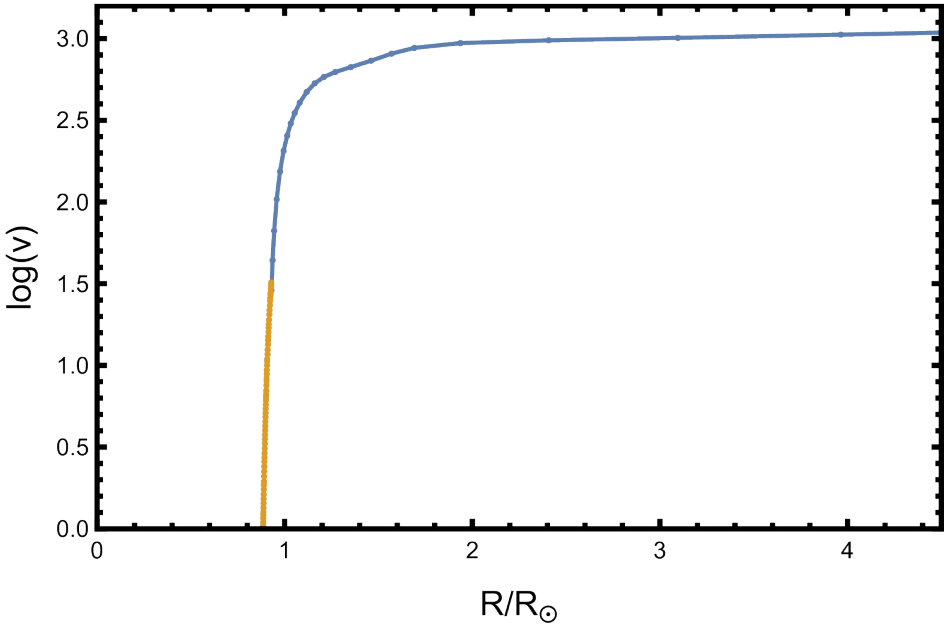
log(v)
3.0
2.5
2.0
1.5
1.0
0.5
0.0
0
1
2
3
4
R/R⊙

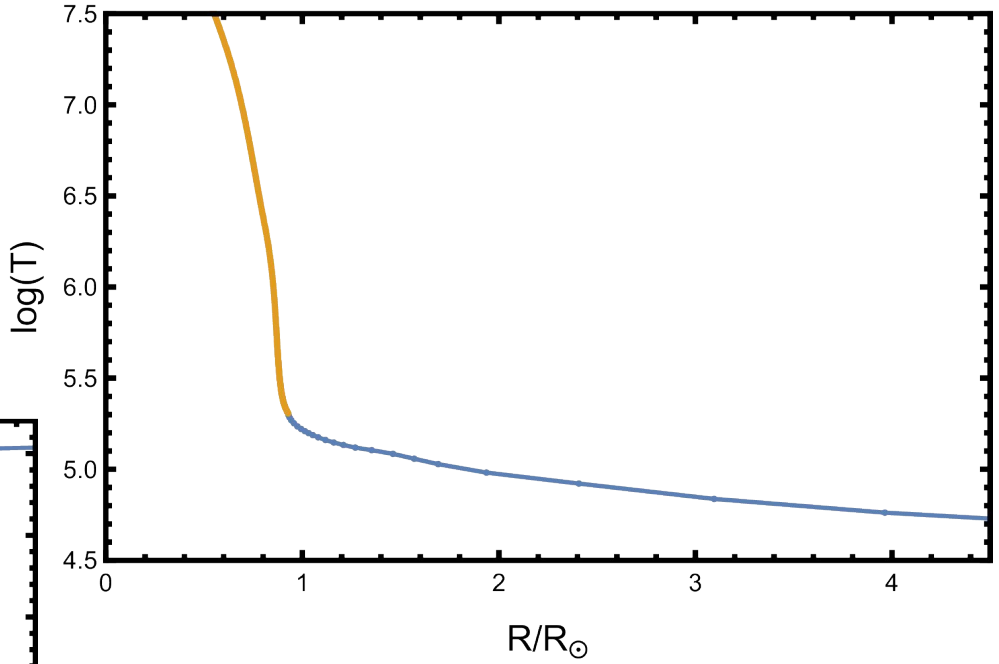
log(T)
7.5
7.0
6.5
6.0
5.5
5.0
4.5
0
1
2
3
4
R/R⊙

Inflation

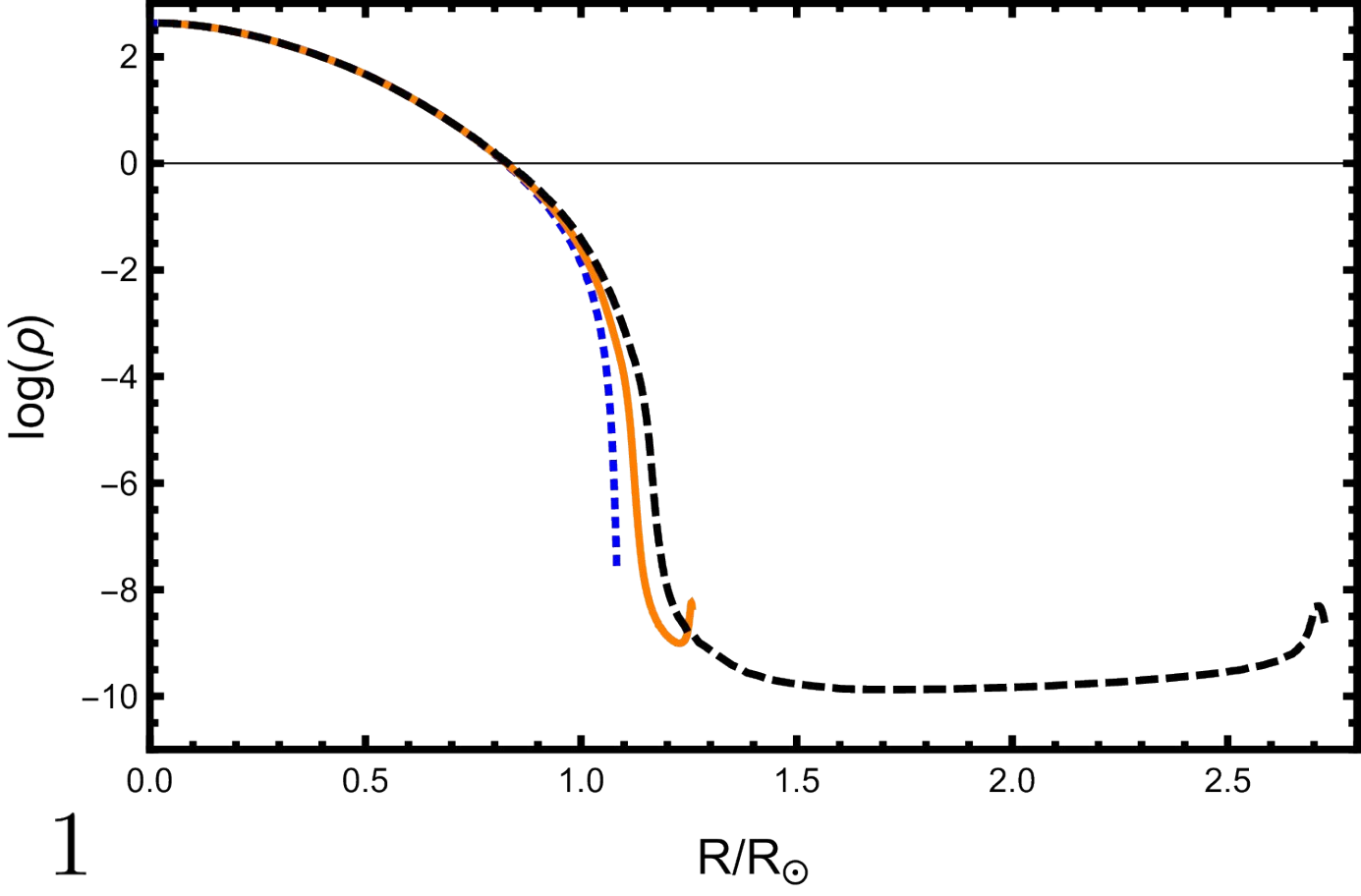

$$\frac{d\log\kappa}{d\log T} < 1 - \frac{1}{\Gamma}$$

20 & 10 Msun

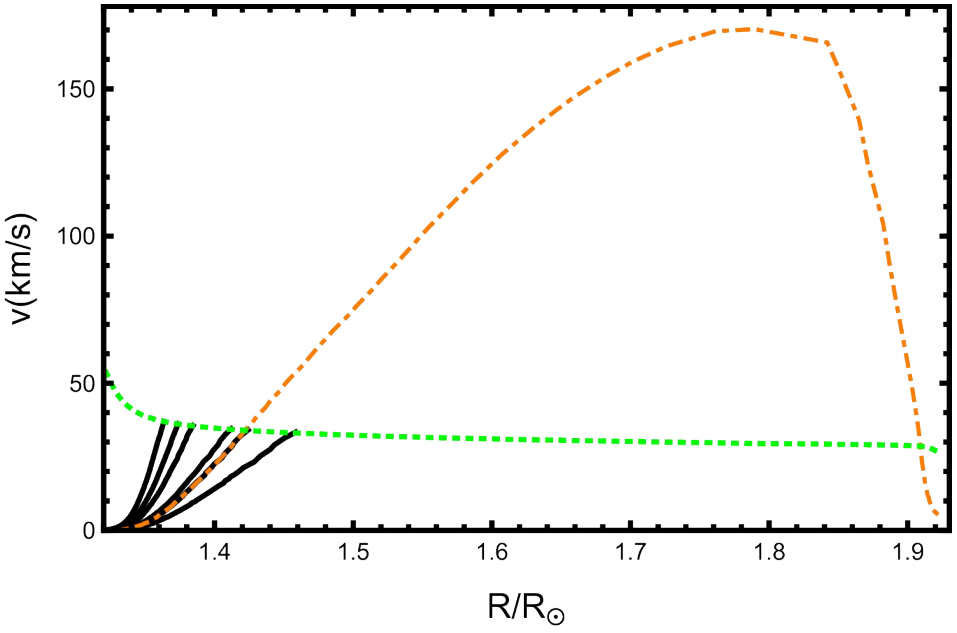
v(km/s)
150
100
50
0
1.4
1.5
1.6
1.7
1.8
1.9
R/R⊙

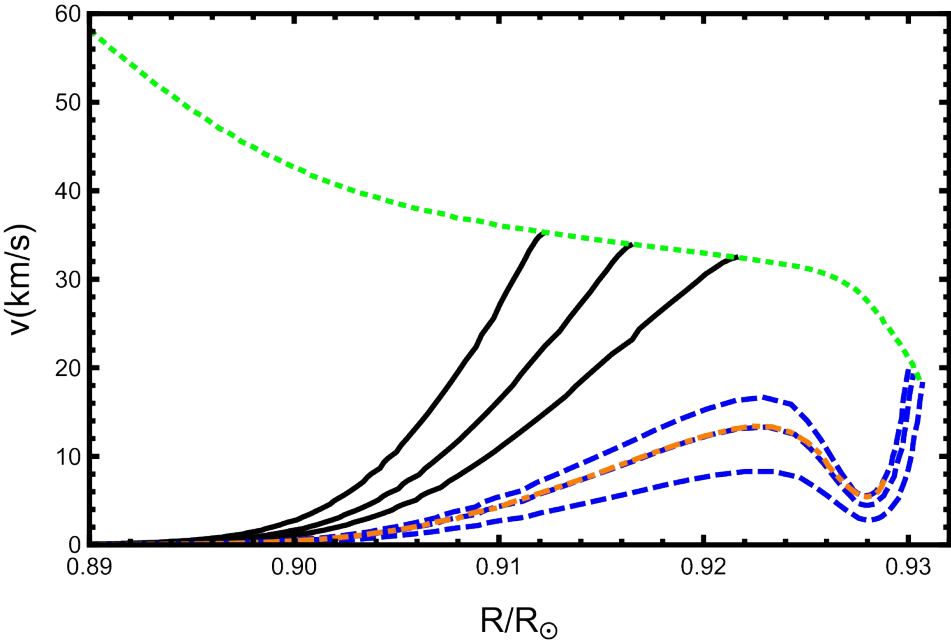
v(km/s)
60
50
40
30
20
10
0
0.89
0.90
0.91
0.92
0.93
R/R⊙

Ts-Mdot diagram

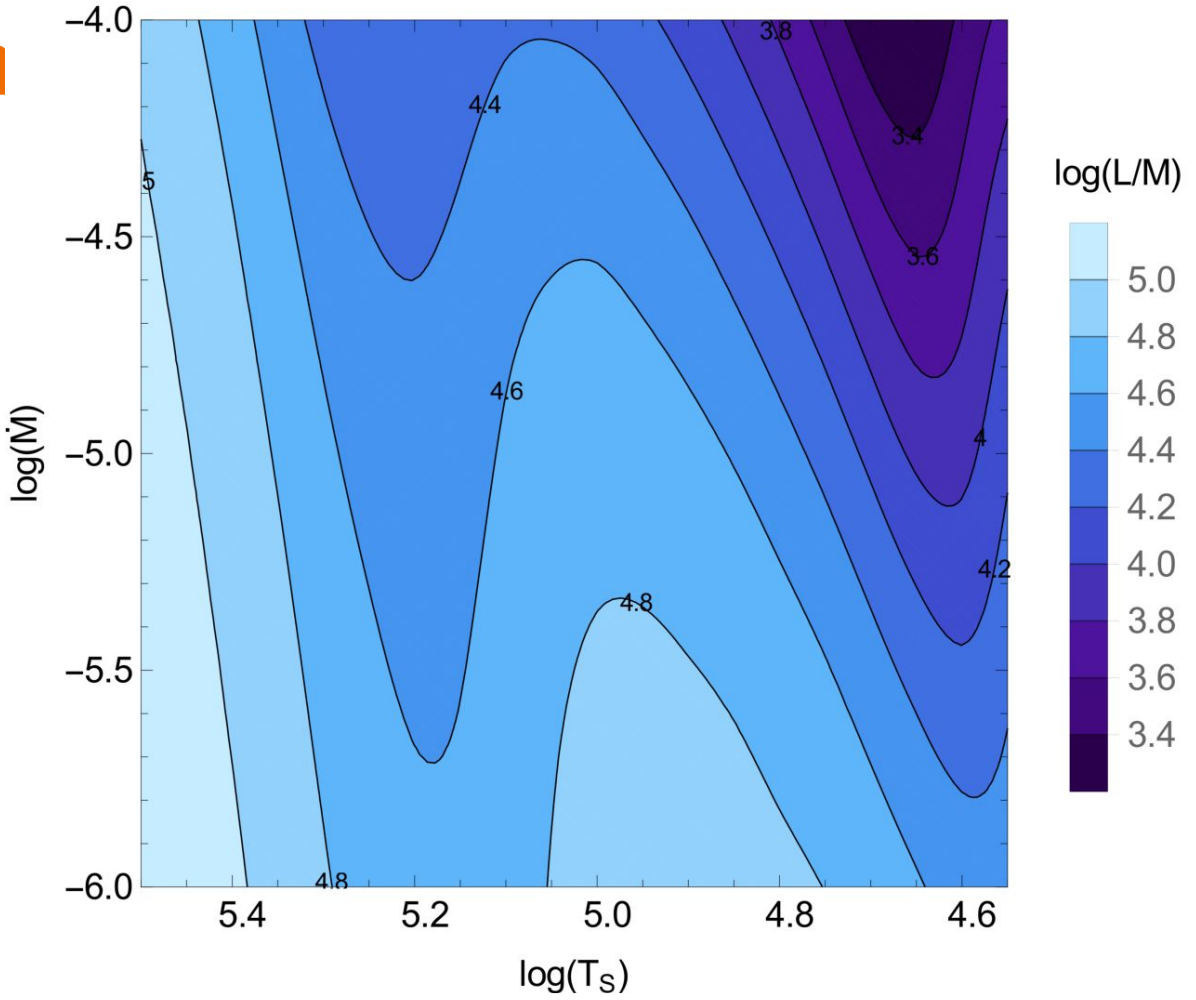

Table A1: Sonic point properties of our set of chemically homogeneous helium star models with mass 15 $M_\odot$ (cf. Sect.4.1)

$\log(\dot{M})$	R_s	$\log(L/L_\odot)$	κ	$\log(\rho_S)$	$\log(T_S)$	$\log(\lambda)$	υ	Γ	t	$\log(H_P)$	$\log(T_{eff})$	τ
$M_\odot/yr$	$R_\odot$		cm^2/g	g/cm^3	K	cm	km/s			cm	K	
-4.3	1.152	5.460	0.6953	-7.967	5.324	8.125	36.23	1.016	18.31	9.185	5.096	33
-4.52	1.159	5.463	0.6834	-8.185	5.304	8.35	35.41	1.010	15.97	9.324	5.095	19
-4.7	1.167	5.465	0.6856	-8.357	5.285	8.521	34.63	1.011	10.49	9.423	5.094	13
-5.0	1.184	5.467	0.6739	-8.655	5.254	8.827	33.43	1.006	8.564	9.609	5.092	7
-5.1	1.194	5.467	0.6773	-8.752	5.239	8.921	32.86	1.005	7.340	9.652	5.090	5
-5.3	1.219	5.468	0.6682	-8.958	5.205	9.133	31.61	1.001	10.79	9.742	5.086	3
-5.4	1.26	5.470	0.7048	-8.833	4.705	8.985	17.76	1.018	0.2025	7.748	5.079	2

Table A2: Same as Table 1 but for our set of models with mass 10 $M_\odot$

$\log(\dot{M})$	R_s	$\log(L/L_\odot)$	κ	$\log(\rho_S)$	$\log(T_S)$	$\log(\lambda)$	υ	Γ	t	$\log(H_P)$	$\log(T_{eff})$	τ
$M_\odot/yr$	$R_\odot$		cm^2/g	g/cm^3	K	cm	km/s			cm	K	
-4.3	0.9121	5.129	0.9804	-7.75	5.295	7.759	35.06	1.009	37.01	8.84	5.064	49
-4.52	0.9164	5.131	0.9712	-7.961	5.264	7.974	33.84	1.006	28.99	8.925	5.064	26
-4.7	0.9216	5.133	0.9602	-8.124	5.228	8.141	32.46	0.9991	34.12	8.946	5.063	16
-5.0	0.9300	5.136	0.9785	-8.213	4.788	8.222	19.55	0.966	0.8827	7.485	5.062	8
-5.1	0.9302	5.137	0.9919	-8.299	4.766	8.302	19.05	0.9647	0.7542	7.474	5.062	6
-5.3	0.9307	5.137	1.0200	-8.481	4.722	8.472	18.10	1.000	0.3659	7.461	5.062	3

Table A3: Same as Table 1 but for our set of models with mass 20 $M_\odot$

$\log(\dot{M})$	R_s	$\log(L/L_\odot)$	κ	$\log(\rho_S)$	$\log(T_S)$	$\log(\lambda)$	υ	Γ	t	$\log(H_P)$	$\log(T_{eff})$	τ
$M_\odot/yr$	$R_\odot$		cm^2/g	g/cm^3	K	cm	km/s			cm	K	
-4.3	1.364	5.678	0.5581	-8.122	5.341	8.376	36.95	1.016	13.03	9.425	5.114	27
-4.52	1.374	5.679	0.5552	-8.342	5.322	8.597	36.17	1.013	9.419	9.575	5.113	16
-4.7	1.385	5.680	0.5528	-8.517	5.308	8.775	35.56	1.010	8.020	9.697	5.111	11
-5.0	1.412	5.681	0.5501	-8.822	5.281	9.081	34.48	1.006	6.444	9.909	5.107	6
-5.1	1.424	5.682	0.5494	-8.922	5.272	9.182	34.13	1.005	5.858	9.980	5.105	2
-5.3	1.458	5.682	0.5476	-9.137	5.252	9.398	33.37	1.003	5.200	10.14	5.100	1